Drebrin contains a cryptic F-actin–bundling activity regulated by Cdk5 phosphorylation

Daniel C. Worth, Catherine N. Daly, Sara Geraldo, Fazal Oozeer, and Phillip R. Gordon-Weeks

Medical Research Council (MRC) Centre for Developmental Neurobiology, King's College London, London SE1 1UL, England, UK

Drebrin is an actin filament (F-actin)–binding protein with crucial roles in neuritogenesis and synaptic plasticity. Drebrin couples dynamic microtubules to F-actin in growth cone filopodia via binding to the microtubule-binding +TIP protein EB3 and organizes F-actin in dendritic spines. Precisely how drebrin interacts with F-actin and how this is regulated is unknown. We used cellular and in vitro assays with a library of drebrin deletion constructs to map F-actin binding sites. We discovered two domains in the N-terminal half of drebrin—a coiled-coil domain and a helical domain—that independently bound to F-actin and cooperatively bundled F-actin. However, this activity was repressed by an intramolecular interaction relieved by Cdk5 phosphorylation of serine 142 located in the coiled-coil domain. Phospho-mimetic and phospho-dead mutants of serine 142 interfered with neuritogenesis and coupling of microtubules to F-actin in growth cone filopodia. These findings show that drebrin contains a cryptic F-actin–bundling activity regulated by phosphorylation and provide a mechanistic model for microtubule–F-actin coupling.

Introduction

Drebrin is an F-actin–binding protein highly expressed in growth cones of developing neurons and in dendritic spines of mature neurons (Ivanov et al., 2009; Dun and Chilton, 2010). Drebrin has roles in neural development, particularly in neuronal migration and neuritogenesis (Geraldo et al., 2008; Mizui et al., 2009; Dun et al., 2012), and in the adult nervous system, where it is involved in the reorganization of actin filaments in dendritic spines underlying memory (Hayashi and Shirao, 1999; Kobayashi et al., 2004; Aoki et al., 2009; Kojima et al., 2010). There is a precipitous loss of drebrin from dendritic spines that occurs before the loss of synapses in people with mild cognitive impairment (Counts et al., 2012), Alzheimer's disease (Harigaya et al., 1996; Hatanpää et al., 1999; Shim and Lubec, 2002), and Down's syndrome (Shim and Lubec, 2002), as well as in mouse models of Alzheimer's disease (Lee and Aoki, 2012). There is experimental evidence that drebrin loss is causal to memory loss (Kobayashi et al., 2004; Kojima et al., 2010).

We have recently shown that drebrin in growth cones links dynamic microtubules to actin filaments in filopodia by binding to the microtubule-binding +TIP protein EB3 (Geraldo et al., 2008). Disruption of this interaction in embryos and cultured neurons, by drebrin knockdown or dominant-negative EB3 constructs, leads to an inhibition of neuronal migration and neuritogenesis (Geraldo et al., 2008; Mizui et al., 2009; Dun et al., 2012). An interaction between drebrin and EB3 that links F-actin to microtubules has been independently confirmed in polarizing epithelial cells (Bazellières et al., 2012) and most probably occurs in dendritic spines, where knockdown of EB3 on invading microtubules has been shown to alter F-actin and spine shape (Jaworski et al., 2009). This suggests that the drebrin–EB3 pathway is canonical.

Drebrin is thought to bind to the side of single actin filaments; however, information about precisely how drebrin interacts with actin filaments and how binding is regulated is lacking. Expression of drebrin in heterologous cells induces filopodia (Shirao et al., 1992, 1994; Hayashi and Shirao, 1999; Hayashi et al., 1999; Keon et al., 2000; Chew et al., 2005; Geraldo et al., 2008), about a third of which contain microtubules

Correspondence to Phillip R. Gordon-Weeks: phillip.gordon-weeks@kcl.ac.uk

S. Geraldo's present address is Equipe de Migration et Invasion Cellulaire, UMR 144, Centre National de la Recherche Scientifique/Institut Curie, 75248 Paris Cedex 05, France.

Abbreviations used in this paper: ADFH, actin-depolymerizing factor homology; BB, blue box; CC, coiled-coil; Hel, helical; LC-MS/MS, liquid chromatography tandem mass spectrometry; mAb, monoclonal antibody; pAb, polyclonal antibody; PP, proline-rich region; Tzone, transition zone.

The Rockefeller University Press $30.00
J. Cell Biol. Vol. 202 No. 5 793–806
www.jcb.org/cgi/doi/10.1083/jcb.201303005

(Geraldo et al., 2008); this proportion nearly doubles when the microtubule-binding +TIP protein EB3 is cotransfected (Geraldo et al., 2008). This induction of filopodia and the ability to capture microtubules might depend on different domains within drebrin.

We conducted a structure–function analysis of drebrin domains by screening a library of contiguous and overlapping drebrin deletion constructs for filopodia induction in heterologous cells. We identified two adjacent F-actin–binding domains in the N-terminal half of drebrin that are responsible for filopodia induction. Using in vitro F-actin cosedimentation assays we showed that these two domains can separately bind F-actin and can act cooperatively to bundle F-actin. We discovered an intramolecular mechanism whereby one F-actin–binding domain is occluded by a domain in the C-terminal half of the protein, and showed that phosphorylation of drebrin by cyclin-dependent kinase 5 (Cdk5) relieves this intramolecular occlusion. Cdk5 phosphorylation of drebrin might target it to parallel F-actin bundles, such as those in growth cone filopodia, and position the molecule appropriately for microtubule capture.

Results

Structure–function analysis of drebrin identifies two F-actin–binding domains

Using an in silico analysis to identify drebrin domains, we found: an N-terminal actin-depolymerizing factor homology (ADFH) domain, which has previously been identified (Larbolette et al., 1999; Kessels et al., 2000; Xu and Stamnes, 2006), followed by a coiled-coil (CC) domain, a helical (Hel) domain, a proline-rich region (PP), and, at the C terminus, a large domain with no identified homology, we named the blue box (BB; Fig. 1 A).

To identify domains involved in filopodia formation we generated a library of contiguous and overlapping drebrin deletion constructs based on our in silico analysis, fused them to YFP at their C terminus, and transfected cDNA encoding them into COS-7 cells (Fig. 1, B–E). To visualize F-actin, we labeled COS-7 cells with phalloidin (Fig. 1, B–E). COS-7 cells transfected with YFP alone were rounded with few processes and the YFP was uniformly distributed throughout the cell (Fig. 1 B). Transfection of cells with drebrin-YFP strongly induced filopodia, as reported previously (Shirao et al., 1992, 1994; Keon et al., 2000; Chew et al., 2005; Geraldo et al., 2008; Fig. 1 C). Both the CC (Fig. 1 D) and the Hel (not depicted) domains were able to independently induce filopodia, confirming previous domain analyses of drebrin in heterologous cells (Hayashi et al., 1999; Xu and Stamnes, 2006; Biou et al., 2008). We quantified this effect by determining the number of filopodia per unit length of cell perimeter (Fig. 1 F). This showed that the CC and Hel domains were almost as efficient as full-length drebrin in eliciting filopodia (Fig. 1 F). There was no additive effect on filopodia numbers when the CC and Hel domains were combined (Fig. 1, E and F). The PP-BB and BB constructs did not induce filopodia (Fig. 1 F; and Fig. S1, A and B). The Abp1 ADFH domain has the closest sequence homology to the ADFH domain in drebrin and binds to F-actin (Lappalainen et al., 1998; Kessels et al., 2000; Goode et al., 2001; Quintero-Monzon et al., 2005). However, when expressed in COS-7 cells, the drebrin ADFH domain was diffusely distributed throughout the cell and did not induce filopodia (Fig. S1 C), which is consistent with previous drebrin domain studies (Hayashi et al., 1999; Chew et al., 2005; Xu and Stamnes, 2006; Grintsevich et al., 2010). Conversely, deleting the ADFH domain from drebrin did not affect filopodia formation in COS-7 cells (Fig. 1 F). Addition of the ADFH domain to the CC and Hel domains or its removal from full-length drebrin did not affect filopodia formation (Fig. 1 F and Fig. S1 D). Addition of the PP and BB domains completely suppressed the induction of filopodia by the Hel domain but not by the CC-Hel domains, which suggests the presence of an autoinhibitory function (Fig. 1 F). The distribution of drebrin constructs within COS-7 cells varied. Those constructs that strongly induced filopodia (ADFH-CC, ADFH-CC-Hel, CC, Hel, and CC-Hel) were concentrated in F-actin–enriched structures such as filopodia and stress fibers, which suggests that they bind F-actin, whereas all of the other constructs were diffusely distributed throughout the cytoplasm (Fig. 1, B–E; and Fig. S1).

Expression of drebrin, or the CC, Hel, or CC-Hel domains, in COS-7 cells appeared to increase the levels of F-actin when compared with YFP, as judged by phalloidin fluorescence (Fig. 1, B–E). Quantification of F-actin levels using phalloidin fluorescence intensity confirmed this observation and showed that drebrin, the CC domain, and CC-Hel construct increased F-actin levels by more than twofold, whereas the Hel domain increased F-actin levels by slightly less than twofold (Fig. 1 G). Overexpression of drebrin in embryonic hippocampal neurons in culture increases F-actin levels in growth cones without changing the overall levels of actin (Mizui et al., 2009). Conversely, knockdown of drebrin in embryonic cortical neurons in culture reduces F-actin in growth cones (Mizui et al., 2009). These findings suggest that drebrin stabilizes F-actin.

To independently confirm that drebrin has two separate F-actin–binding domains, we used an in vitro F-actin cosedimentation assay (Fig. 2). Actin filaments were incubated with recombinant drebrin proteins in an actin assembly buffer and then centrifuged at low speed to pellet bundled F-actin, and the resulting supernatant was centrifuged at high speed to pellet individual actin filaments. When His-tagged drebrin was incubated with F-actin, actin was recovered, along with drebrin, in both the low- and high-speed pellets (Fig. 2 A). Because drebrin incubated without F-actin did not pellet under these conditions (Fig. 2 A), this experiment suggests that drebrin bundles F-actin and confirms that drebrin binds to single actin filaments (Fig. 2 A). In contrast, when F-actin was incubated with either the CC (Fig. 2 B) or the Hel (Fig. S2 A) domain, F-actin did not pellet after low-speed centrifugation but was recovered in the high-speed pellets along with the CC or Hel domain, which suggests that although the CC and Hel domains cannot bundle F-actin they can bind to actin filaments, confirming the in vivo findings (Fig. 2 B). F-actin bundling requires the cooperative action of at least two F-actin–binding domains. To test whether the CC and the Hel domains acting together might be responsible for F-actin bundling by drebrin, we assessed the ability of the CC-Hel construct to bundle F-actin. When the CC-Hel construct was incubated with F-actin, we found that it was recovered,

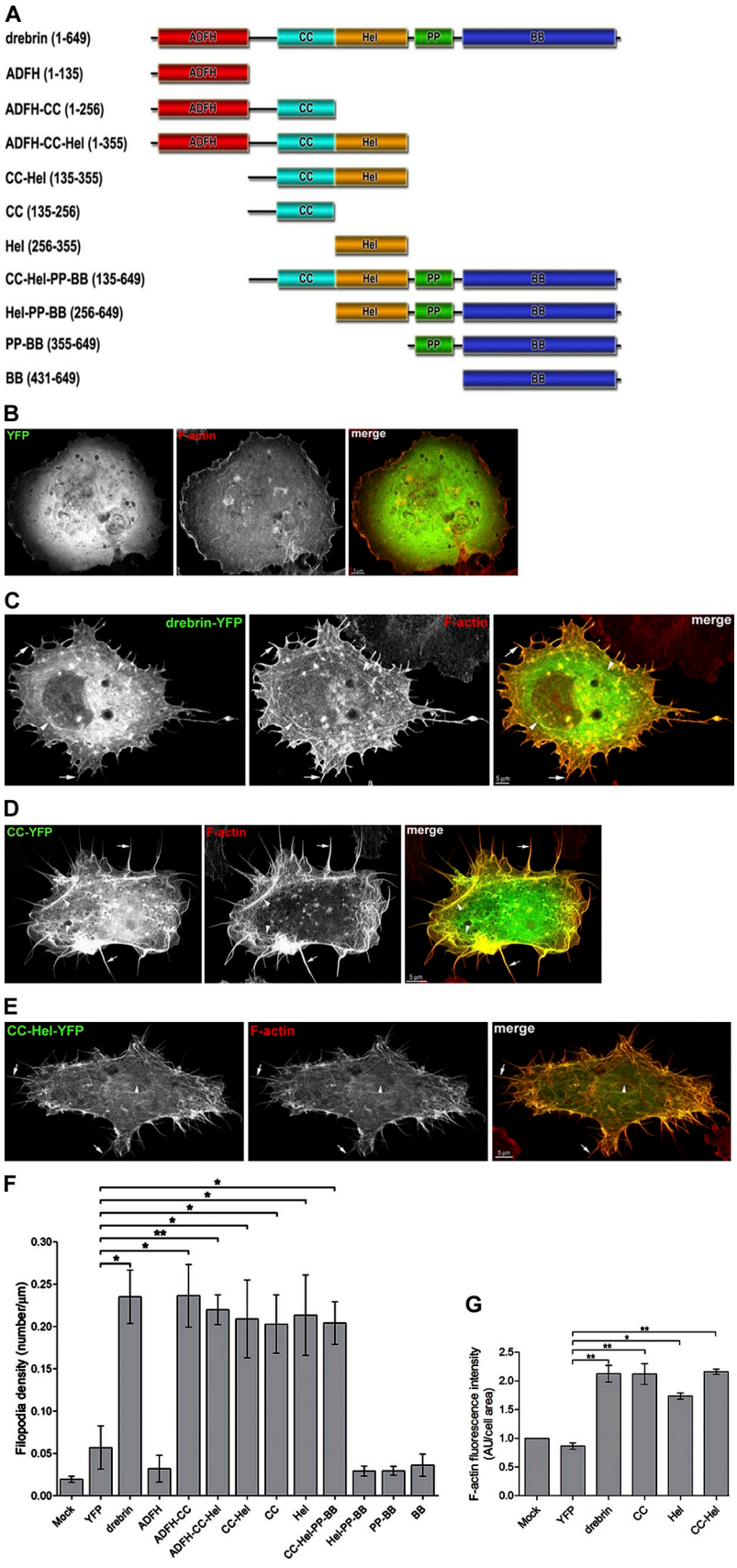

Figure 1. **Drebrin contains two F-actin–binding domains responsible for filopodia formation in heterologous cells.** (A) Domain diagrams of drebrin and drebrin deletion constructs used for the functional domain analysis of drebrin. Drebrin has five potential functional domains identified by an in silico analysis using InterPro, Pfam, SMART, and PROSITE. Constructs are YFP-tagged at the C terminus. ADFH, actin-depolymerizing factor homology domain (red, residues 1–135); CC, coiled-coil domain (turquoise, residues 176–256); Hel, helical domain (orange, residues 256–355); PP, proline-rich region (green, residues 364–417); BB, blue box, drebrin C-terminal region (blue, residues 431–649). Numbering is for human drebrin E. (B–E) Immunofluorescence confocal images of COS-7 cells transfected with cDNA encoding YFP-tagged drebrin and drebrin deletion constructs (green) and labeled with phalloidin for F-actin (red). Bars, 5 µm. (B) COS-7 cells expressing YFP alone are rounded and have few processes. The YFP protein is diffusely distributed throughout the cell. (C) Drebrin-YFP expression in COS-7 cells induces F-actin–rich filopodia containing drebrin-YFP (arrows). Drebrin-YFP also localizes to stress fibers (arrowheads). (D and E) CC-YFP (D) or CC-Hel-YFP (E) expression in COS-7 cells also induces F-actin rich filopodia (arrows). The CC-YFP (D) and the CC-Hel-YFP (E) protein localize to filopodia (arrows) and to stress fibers (arrowheads). (F) The CC and Hel domains of drebrin induce filopodia to the same extent as the full-length protein. Shown is a quantification of the number of filopodia per unit length of cell perimeter (filopodia density) in COS-7 cells. Expression of drebrin deletion constructs that contain the CC, the Hel, or both domains, including full-length drebrin, significantly increases the density of filopodia. Surprisingly, filopodia formation induced by the Hel domain is suppressed in the Hel-PP-BB deletion construct. Mock, mock transfection; YFP, YFP alone transfection. Values are mean ± SEM (error bars) of at least 10 cells per transfection from three independent experiments. Significant differences (unpaired Student's *t* test): *, $P < 0.05$; **, $P < 0.01$). (G) Drebrin and the CC and Hel domains increase F-actin levels in transfected COS-7 cells. Shown is a quantification of the F-actin levels in COS-7 cells transfected with various constructs. F-actin levels were quantified by measuring the intensity of phalloidin fluorescence in single confocal optical planes of COS-7 cells at the level of stress fibers and dividing this by the area of the cell. Values are mean ± SEM (error bars) of at least 10 cells per transfection from two or three independent experiments. Significant differences (unpaired Student's *t* test): *, $P < 0.001$; **, $P < 0.0001$.

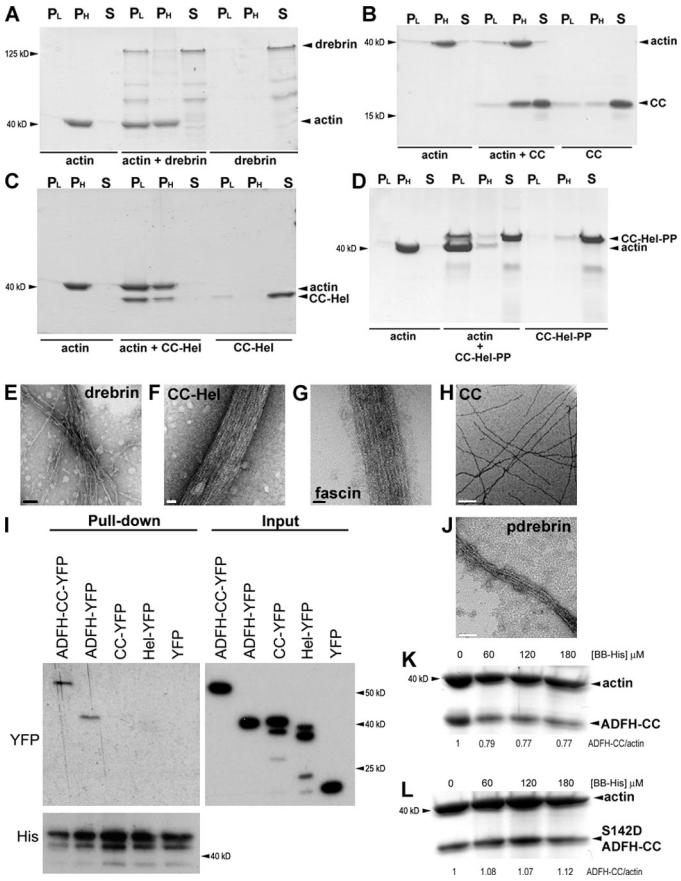

Figure 2. **In vitro F-actin cosedimentation assays show that drebrin is an F-actin–bundling protein and confirm the presence of separate F-actin binding in the CC and Hel domains.** Actin filaments were incubated with or without recombinant drebrin proteins and F-actin bundles/meshes pelleted by low speed centrifugation (P_L). The resulting supernatant was then centrifuged at high speed to pellet single actin filaments (P_H). The supernatants from the high-speed centrifugation (S), P_L, and P_H were analyzed by gel electrophoresis and Coomassie blue staining. (A) Drebrin bundles and binds to F-actin. Actin filaments pellet after high-speed centrifugation (P_H) but do not pellet after low-speed centrifugation (P_L). Addition of drebrin results in the appearance of actin in the low-speed pellet (P_L) together with a small amount of drebrin as well as in the high-speed pellet (P_H). Drebrin alone does not pellet under either condition. (B) The CC domain binds but does not bundle F-actin. When added to F-actin, the CC construct appears in the high-speed pellet (P_H) but not the low-speed pellet (P_L). The CC construct alone does not pellet under either condition. (C) The CC-Hel domain construct is a strong F-actin bundler. When added to F-actin, the CC-Hel construct appears in both the high-speed pellet (P_H) and the low-speed pellet (P_L). The CC-Hel construct alone does not pellet under either condition. (D) Addition of the PP domain has little effect on the bundling activity of the CC-Hel domains. When added to F-actin, the CC-Hel-PP construct appears in both the high-speed pellet (P_H) and the low-speed pellet (P_L). The CC-Hel-PP construct alone does not pellet under either condition. (E–H) Electron micrographs of negatively stained F-actin from in vitro F-actin cosedimentation assays after addition of drebrin or drebrin deletion constructs. (E) After the addition of drebrin, thin, loose bundles of F-actin are visible. Bar, 50 nm. (F) After the addition of the CC-Hel construct, thick, tight bundles of F-actin are visible. Bar, 20 nm. (G) After the addition of fascin, a thick, tight bundle of F-actin is visible. Bar, 20 nm. (H) After the addition of the CC construct, single actin filaments are seen and there are no bundles of F-actin. Bar, 200 nm. (I) The BB domain binds to the ADFH domain. An immunoblot of YFP-tagged proteins, identified with GFP antibody, in BB-His pull-downs (Pull-down) is shown. Cell extracts of COS-7 cells expressing drebrin deletion constructs (Input) were mixed with recombinant BB-His and proteins bound to nickel beads separated by SDS-PAGE and transferred to PVDF membranes. Blots were probed with GFP and His-tag antibodies. (J) Electron micrograph of negatively stained F-actin from an in vitro F-actin cosedimentation assay after addition of drebrin that had been preincubated with a neonatal rat brain extract. A thin, tight bundle of F-actin is visible. Bar, 50 nm. (K) The BB domain inhibits binding of the ADFH-CC construct to F-actin. Actin filaments were incubated with the His-tagged ADFH-CC construct in the absence or presence of increasing concentrations ([BB-His] μM) of the His-tagged BB domain. The ratio of His-tagged ADFH-CC to actin is shown (ADFH-CC/actin). (L) The BB domain does not inhibit binding of the S142D ADFH-CC construct to F-actin. Actin filaments were incubated with the His-tagged S142D ADFH-CC construct in the absence or presence of increasing concentrations ([BB-His] μM) of the His-tagged BB domain. The ratio of His-tagged ADFH-CC to actin is shown (ADFH-CC/actin).

along with F-actin, in both low- and high-speed pellets, which suggests that the CC and Hel domains bind to actin filaments and cooperate to bundle F-actin (Fig. 2 C).

To confirm that drebrin and the CC-Hel domain construct can bundle F-actin, we examined F-actin morphology by negative-staining EM (Fig. 2, E and F). Recombinant His-tagged drebrin mainly produced an unorganized meshwork of F-actin and only occasional loose F-actin bundles with an interfilament distance of 12.02 ± 0.56 nm (mean ± SEM) and, on average, 4.90 ± 0.18 (mean ± SEM) actin filaments per bundle that were aligned only over short distances (Fig. 2 E), which suggests that recombinant His-tagged drebrin is, at best, a weak F-actin bundler. In contrast, the recombinant CC-Hel construct produced tight F-actin bundles with an interfilament distance of 7.81 ± 0.06 nm (mean ± SEM) and, on average, 10.7 ± 1.08 (mean ± SEM) filaments per bundle that were aligned over considerable distances (Fig. 2 F). Thus, the CC-Hel domain construct bundled F-actin far more effectively than drebrin. We compared the F-actin bundling activity of the CC-Hel construct with fascin, an established F-actin bundler (Jansen et al., 2011; Fig. 2 G). Fascin, as expected, produced tight F-actin bundles with an interfilament distance of 8.81 ± 0.12 nm (mean ± SEM) and, on average, 8.46 ± 0.63 (mean ± SEM) filaments per bundle. This is similar to what has been reported previously (Ishikawa et al., 2003; Jansen et al., 2011) and to the CC-Hel construct reported here. The CC (Fig. 2 H) and the Hel (not depicted) domain constructs did not produce F-actin bundles, which suggests that F-actin binding by these constructs is sufficient to induce filopodia in COS-7 cells (Fig. 1, D and F). To assess whether the ADFH domain is involved in F-actin bundling or binding, we also tested the His-tagged ADFH drebrin deletion construct in the F-actin cosedimentation assay. This showed that drebrin lacking the ADFH domain can bind and weakly bundle F-actin, similar to full-length drebrin (Fig. S2, B and C).

An intramolecular interaction represses drebrin F-actin bundling

When expressed in COS-7 cells, drebrin and the CC-Hel construct were equally efficient at inducing filopodia, and hence presumably bundling F-actin, whereas EM analysis in the F-actin in vitro cosedimentation assay showed that recombinant drebrin was a weak F-actin bundler, while the CC-Hel construct strongly bundled F-actin (Figs. 1 and 2). One explanation for this disparity is that the F-actin bundling activity of drebrin,

which depends on the concerted actions of the CC and Hel domains, is cryptic in full-length recombinant drebrin but exposed when drebrin is expressed in eukaryotic cells. Inhibition of the F-actin bundling activity might occur if a region of drebrin outside the CC and Hel domains masked an F-actin binding site. The cosedimentation assay result with the ADFH deleted drebrin suggests that the ADFH domain is not involved in intramolecular masking (Fig. S2, B and C). To determine whether the PP or the BB domains are involved we tested the CC-Hel-PP construct in the cosedimentation assay and found that it strongly bundled F-actin (Fig. 2 D) with an interfilament distance of 8.36 ± 0.16 nm (mean ± SEM), which is similar to the CC-Hel construct, but that there were fewer filaments per bundle (5.48 ± 0.36; mean ± SEM). This result implicates the BB in occluding F-actin bundling activity. To test this idea, we looked for an interaction between the BB and CC-Hel containing constructs. We combined cell extracts from COS-7 cells expressing YFP-tagged drebrin deletion constructs with recombinant His-tagged BB domain and pulled down the BB domain using nickel beads. This showed that the BB domain binds to the ADFH-CC construct and, less strongly, to the ADFH construct, but not to the CC or Hel domains (Fig. 2 I). This suggests that the BB binding domain occludes an F-actin–binding domain in drebrin indirectly by binding to drebrin at the ADFH–CC border. To test the prediction that intramolecular binding of the BB domain to the ADFH–CC border occludes F-actin binding, we performed an in vitro cosedimentation assay with His-tagged ADFH-CC in the presence of increasing concentrations of His-tagged BB. This showed that the BB domain can inhibit binding of the CC domain to F-actin (Fig. 2 K).

Phosphorylation of drebrin at S142 regulates F-actin bundling

Drebrin is a phosphoprotein (Ballif et al., 2004; Chew et al., 2005; Collins et al., 2005), and one potential difference between bacterially expressed recombinant drebrin and drebrin expressed in eukaryotic cells is phosphorylation. To test for a role of phosphorylation in regulating F-actin bundling activity, we exposed recombinant His-tagged drebrin to a neonatal brain extract in a kinase buffer containing ATP, affinity-purified the protein, and then tested it in the in vitro cosedimentation assay. This treatment markedly improved the F-actin bundling activity of recombinant His-tagged drebrin (Fig. S2 D). EM analysis of F-actin bundled by recombinant drebrin exposed to a brain extract revealed F-actin bundles that were similar in morphology to those produced by the CC-Hel construct, although the bundles were thinner (Fig. 2 J). The interfilament distance was 8.32 ± 0.15 nm (mean ± SEM) with, on average, 5 ± 0.19 (mean ± SEM) filaments per bundle.

The His-tagged drebrin that binds to F-actin bundles in the cosedimentation assay after exposure to a brain extract migrates more slowly in SDS PAGE gels than drebrin that binds to single actin filaments. This is consistent with the idea that phosphorylation of drebrin regulates F-actin bundling (Fig. S2 D). We determined the phosphorylation state of drebrin in these different fractions using tandem mass spectrometry. This revealed that drebrin bound to F-actin bundles is phosphorylated either at S141 or S142, whereas drebrin bound to single filaments, or remaining in the supernatant, is not phosphorylated at these sites (Table S1). S141 and S142 are in the CC domain near the border with the ADFH domain and are candidate phosphorylation sites for regulating drebrin F-actin bundling. We raised phospho-specific antibodies to pS141 (pAb pS141) and pS142 (pAb pS142) and used them to confirm that drebrin exposed to a brain extract is phosphorylated at S141 and S142 (Fig. 3 A). However, native drebrin in neonatal brain extracts and drebrin-YFP expressed in COS-7 cells is phosphorylated at S142 but not S141 (Fig. 3 A).

When expressed in COS-7 cells, drebrin-YFP that localizes to filopodia is phosphorylated at S142, as shown by immunolabeling with pAb pS142, whereas drebrin-YFP localized to stress fibers is not (Fig. 3, B and C). In embryonic cortical neurons in culture that have yet to extend neurites (stage I; Dotti et al., 1988), drebrin localizes to the F-actin bundles of actin arcs and to actin filament puncta, and occasionally extends into filopodia (Fig. 3, D–F). Drebrin can be phosphorylated at S142 in filopodia and in actin filament puncta in stage I neurons, but not in actin arcs (Fig. 3, D and E). Furthermore, not all stage I neurons have S142-phosphorylated drebrin despite having similar levels of drebrin to stage I neurons that do have S142-phosphorylated drebrin (Fig. 3 E). In the growth cones of neurons that have extended neurites (stage II and III; Dotti et al., 1988), drebrin is highly concentrated in the transition zone (Tzone), at the border between the central and peripheral domains (Geraldo et al., 2008; Mizui et al., 2009), and in the base of some filopodia (Geraldo et al., 2008; Fig. 3 G). However, drebrin is phosphorylated in the base of filopodia but not in the Tzone (Fig. 3 G), as confirmed by fluorescence intensity analysis (Fig. 3, H and I). Because F-actin is organized in parallel bundles in filopodia, whereas in stress fibers and actin arcs the F-actin is antiparallel, these findings suggest that S142-phosphorylated drebrin can distinguish between parallel and antiparallel F-actin bundles and are consistent with the idea that S142 phosphorylation regulates F-actin bundling. Polyclonal antibodies to pS141 did not label embryonic cortical neurons in culture (Fig. S3).

To determine whether pS142 is required to relieve the intramolecular repression of F-actin bundling, we made phosphomimetic (changing S to D) and phospho-dead (changing S to A) mutants of drebrin S142. When expressed in COS-7 cells, S142D drebrin induced filopodia to a similar extent as drebrin, whereas S142A drebrin was not significantly different from YFP alone (Fig. 4, A and B). S142A drebrin localized to filopodia and stress fibers, but S142D only localized to filopodia, which is consistent with phosphorylation of S142 enabling binding to parallel F-actin bundles (Fig. 4, C and D). Drebrin-YFP expressed in stage I embryonic cortical neurons in culture localized to F-actin puncta, F-actin arcs, and filopodia (not depicted), as do endogenous drebrin (Fig. 3, D–F) and S142D drebrin-YFP (Fig. 4 E), whereas S142A drebrin-YFP localized to F-actin puncta and F-actin arcs but not to filopodia (Fig. 4 E). In growth cones of stage II/III neurons, drebrin-YFP localized to the Tzone and filopodia (Geraldo et al., 2008), as does endogenous drebrin (Fig. 3 G). In contrast, S142A drebrin-YFP was

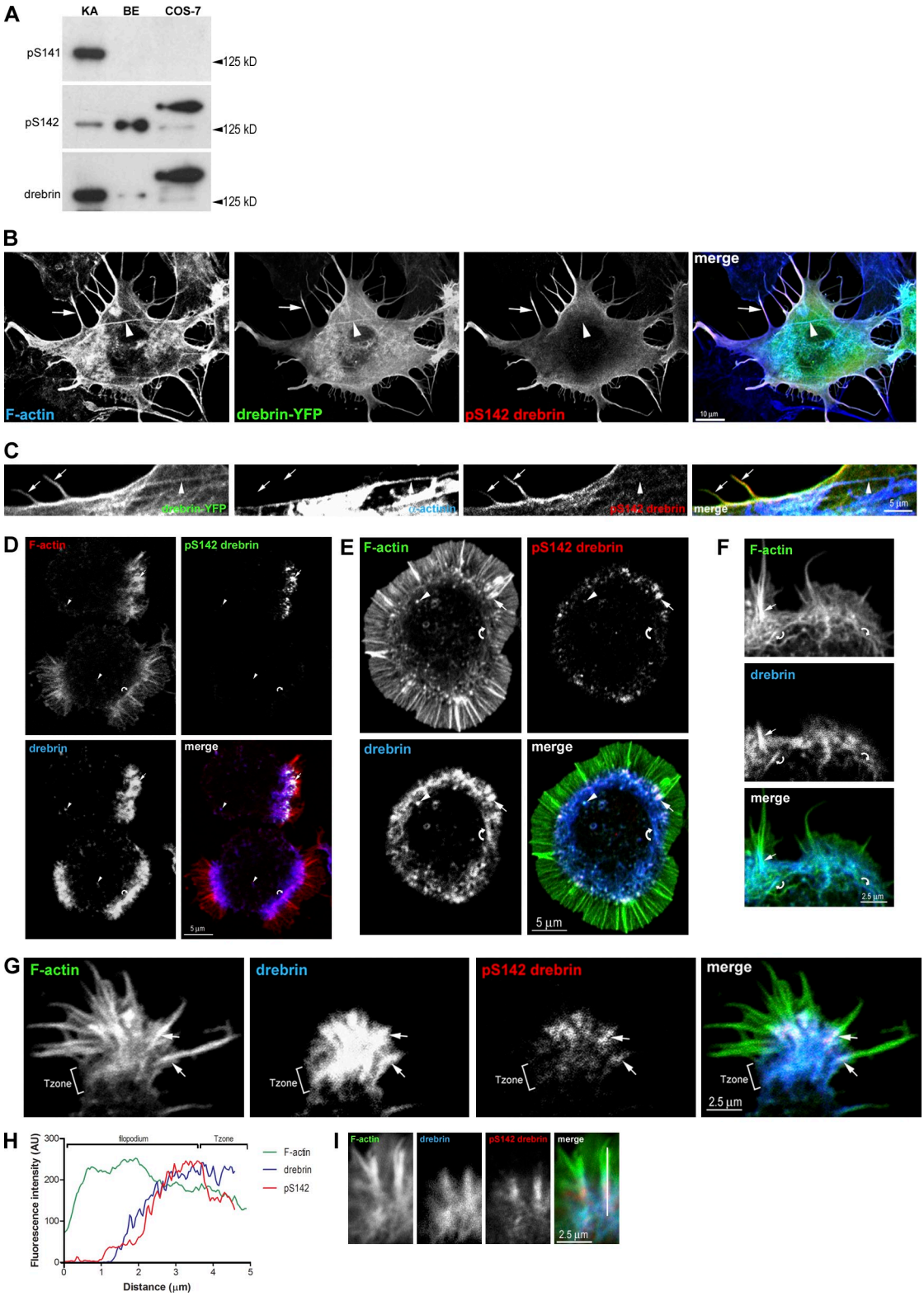

Figure 3. **Drebrin is phosphorylated at S142 when bound to parallel F-actin bundles in filopodia but not when bound to antiparallel F-actin bundles in stress fibers or actin arcs.** (A) His-tagged drebrin exposed to a neonatal rat brain extract in kinase buffer (KA) becomes phosphorylated at S141 and S142, whereas endogenous drebrin in neonatal rat brain extract (BE) and drebrin-YFP expressed in COS-7 cells (COS-7) is phosphorylated at S142 but not S141. Immunoblots were probed with pAb pS141, pAb pS142, and antibody against drebrin. (B and C) Drebrin-YFP phosphorylated at S142 in COS-7 cells localizes to filopodia, where parallel bundles of F-actin are concentrated, but not to stress fibers where antiparallel F-actin bundles are concentrated. Immunofluorescence confocal images of COS-7 cells transfected with cDNA encoding YFP-tagged drebrin (green) and labeled with phalloidin for F-actin (B, blue) or α-actinin to label stress fibers (C, blue) and pAb pS142 (B and C, red). Drebrin-YFP localized to filopodia is phosphorylated at S142 (arrows) but is not phosphorylated at S142 in stress fibers (arrowheads). (D–F) In stage I embryonic cortical neurons in culture, drebrin, phosphorylated at S142, localizes to F-actin puncta and the base of filopodia. Immunofluorescence confocal images of stage I neurons labeled with phalloidin for F-actin and antibodies against

restricted to the Tzone, whereas S142D drebrin-YFP particularly targeted filopodia (Fig. 4 F), as confirmed by fluorescence intensity analysis (Fig. 4, G and H).

In F-actin cosedimentation assays, EM analysis of the S142D mutant showed that it strongly bundled F-actin with an interfilament distance of 8.00 ± 0.11 nm (mean ± SEM), similar to that of the CC-Hel construct, with, on average, 7.18 ± 0.45 (mean ± SEM) filaments per bundle, whereas the S142A mutant weakly bundled F-actin similar to wild-type drebrin (Fig. 4, I and J). Furthermore, as predicted, the BB domain failed to inhibit binding of the His-tagged phosphomimetic S142D ADFH-CC to F-actin (Fig. 2 L). These findings show that pS142 is necessary and sufficient to overcome the intramolecular repression of F-actin bundling by the BB domain.

Cyclin-dependent kinase 5 phosphorylates drebrin at S142

Drebrin S142 is highly conserved in the vertebrates, as is a proline immediately downstream of S142 and arginine at −3 (but not in fish) and at +5 (Table S2). Because these features form the recognition motif for cyclin-dependent kinase 5 (Cdk5) and dual specificity tyrosine phosphorylation–regulated kinase 1A (DYRK1A), we tested whether these kinases could phosphorylate S142 (Songyang et al., 1996). Cdk5 inhibitors, but not DYRK1A inhibitors, reduced pS142 drebrin levels in embryonic cortical cultures (Fig. 5, A and B). Furthermore, cell extracts from embryonic cortical cultures or recombinant Cdk5/p35 phosphorylated recombinant drebrin at S142 in vitro (Fig. 5, C and D). Finally, in vitro phosphorylation of recombinant drebrin at S142 by Cdk5/p35 enhanced F-actin bundling (Fig. 5 E). EM analysis showed that in vitro Cdk5/p35 phosphorylated drebrin produced F-actin bundles with an interfilament distance of 8.01 ± 0.13 nm (mean ± SEM) and, on average, 5.95 ± 0.29 (mean ± SEM) filaments per bundle. This is caused by phosphorylation of S142, as incubation with Cdk5/p35 did not enhance the F-actin bundling activity of S142A drebrin (Fig. 5 F).

To ascertain whether the binding of EB3 to drebrin is altered by S142 phosphorylation, we expressed drebrin-YFP, S142A drebrin-YFP, or S142D drebrin-YFP in COS-7 cells and used an antibody to EB3 to immunoprecipitate endogenous EB3 from cell lysates. Immunoblots probed with a drebrin antibody revealed that drebrin-YFP strongly coimmunoprecipitates with EB3, as expected (Geraldo et al., 2008), as does S142D drebrin-YFP, although to a lesser extent, whereas S142A drebrin-YFP only very weakly coimmunoprecipitates with EB3 (Fig. 5 G). These findings suggest that EB3 preferentially binds to pS142 drebrin.

Phospho-S142 mutants of drebrin alter neuritogenesis and microtubule capture in growth cone filopodia

Previously, we showed that drebrin plays an important role in neuritogenesis and microtubule capture by growth cone filopodia (Geraldo et al., 2008), and so we investigated the role of drebrin serine 142 phosphorylation in these processes using phospho-mimetic and phospho-dead mutants of serine 142.

To assay neuritogenesis, we expressed drebrin-YFP, S142A drebrin-YFP, or S142D drebrin-YFP in cortical neurons, replated the neurons 2 d after transfection to restart neuritogenesis, and labeled fixed neurons with GFP antibody to identify transfected neurons, and with an antibody to microtubules (mAb YL 1/2) to label neurites, 1 h after replating. As a measure of neuritogenesis, transfected neurons were scored for the absence (stage I) or presence (stage II/III) of neurites. We found that neuritogenesis in cultured embryonic cortical neurons was retarded in neurons expressing S142A drebrin-YFP and accelerated in neurons expressing S142D drebrin-YFP compared with neurons expressing drebrin-YFP (Fig. 5, H and I), which implies that F-actin bundling and microtubule coupling by drebrin, regulated by S142 phosphorylation, is important for neuritogenesis. Consistent with this idea, pS142 drebrin accumulates along with dynamic microtubules and F-actin bundles at nascent growth cones in stage I neurons commencing neuritogenesis (Fig. 5 J). Using fluorescence intensity line plots (Fig. 5 K), we found that microtubules are associated with 77 ± 0.02% of filopodia that contain pS142 drebrin (mean ± SEM; n = 32 from three independent experiments).

To assay for microtubule–F-actin interactions in growth cone filopodia, we expressed drebrin-YFP, S142A drebrin-YFP, or S142D drebrin-YFP in cortical neurons and labeled fixed neurons 2 d later with GFP antibody to identify transfected neurons, with mAb YL 1/2 for dynamic microtubules and phalloidin to label filopodia (Fig. 5 L). Expression of wild-type and S142D drebrin in embryonic cortical neurons in culture increased the proportion of growth cone filopodia containing a microtubule, whereas S142A drebrin reduced microtubule association (Fig. 5, L and M). These findings are consistent with a role for S142 phosphorylation in microtubule–F-actin interactions.

Discussion

Drebrin has two F-actin–binding domains that bundle F-actin

Drebrin was thought to have a single F-actin–binding domain that enabled it to bind to the side of actin filaments (Dun and

drebrin and drebrin phosphorylated at S142. Drebrin is present in F-actin puncta (arrowheads, D and E), actin arcs (curved arrows, D–F), and occasionally in the base of filopodia (arrows, D and F). Drebrin is phosphorylated at S142 in the base of filopodia (arrows in D and E) and in F-actin puncta (arrowheads in D), whereas drebrin in actin arcs is not (curved arrows in D–F). (G) Immunofluorescence confocal images of a growth cone from a stage II neuron labeled with phalloidin for F-actin (green) and antibodies against drebrin (blue) and drebrin phosphorylated at S142 (red). Drebrin is phosphorylated at S142 in the base of filopodia (arrows) but not in the Tzone. (H) Fluorescence intensity in arbitrary units (AU) of F-actin (green), drebrin (blue), and pS142 drebrin (red) along the line plot shown in I (merge). pS142 drebrin is mainly localized to the base of the filopodium. Note that the drebrin level in the base of the filopodium is similar to that in the Tzone, showing that drebrin is selectively phosphorylated at the base of the filopodium. (I) Immunofluorescence confocal images from a growth cone labeled with phalloidin for F-actin (green) and antibodies against drebrin (blue) and drebrin phosphorylated at S142 (red). The white line (merge) shows the region used for the fluorescence intensity line plot shown in H. Bars: (B) 10 µm; (C–E) 5 µm; (F, G, and I) 2.5 µm.

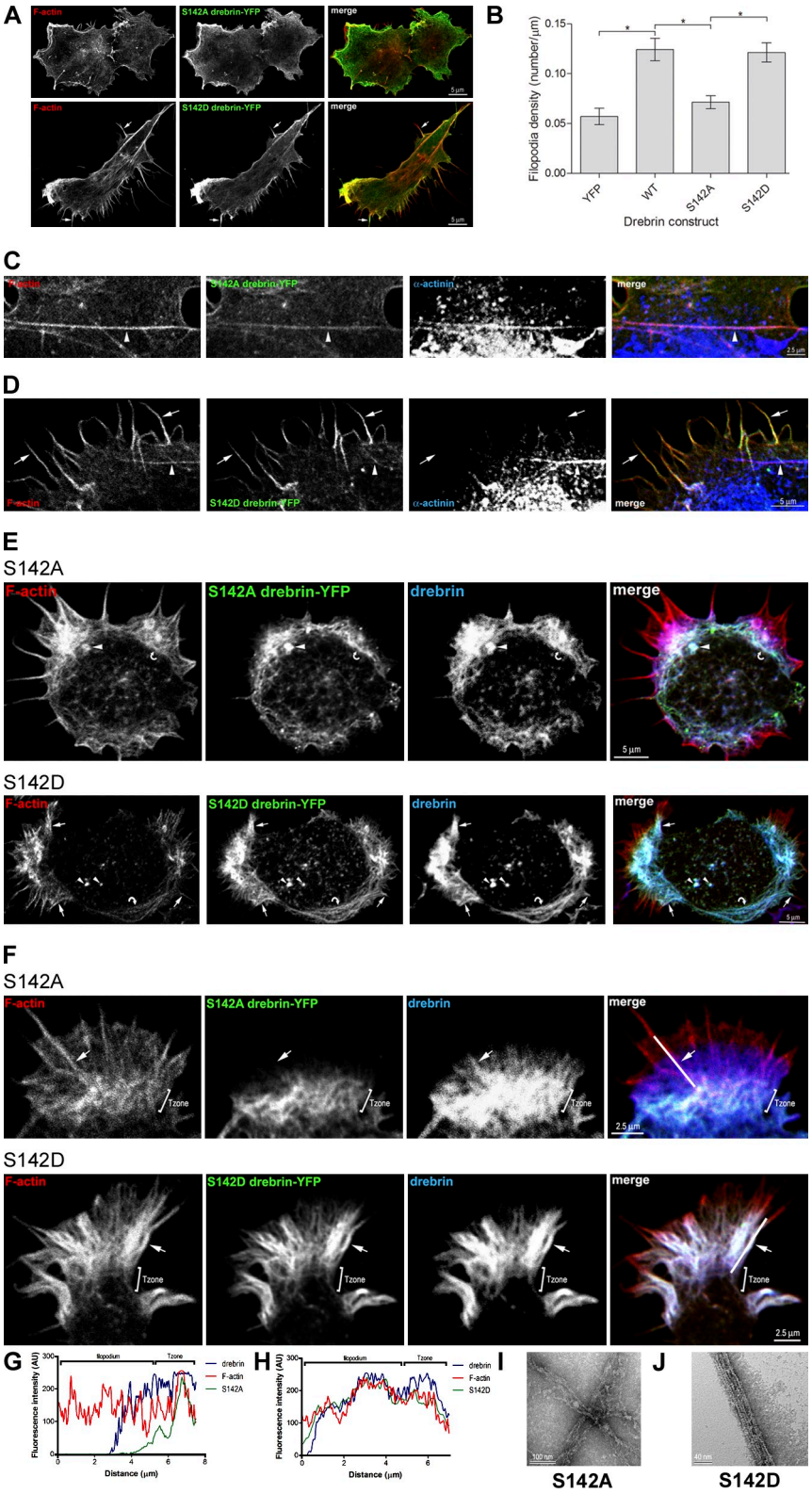

Figure 4. **Phosphorylation of drebrin at S142 is necessary and sufficient to relieve the intramolecular repression of F-actin bundling.** (A) Immunofluorescence confocal images of COS-7 cells transfected with cDNA encoding YFP-tagged drebrin (green) mutated at S142 changing S to A (S142A) or S to D (S142D). Cells were labeled with phalloidin for F-actin (red). S142A drebrin-YFP only weakly induces F-actin containing filopodia, whereas S142D drebrin-YFP strongly induces filopodia (arrows). (B) Quantification of the number of filopodia per unit length of cell perimeter (filopodia density) in COS-7 cells transfected with cDNA encoding YFP, YFP-tagged drebrin (WT), and YFP-tagged drebrin mutated at S142 changing S to A (S142A) or S to D (S142D). Values are mean ± SEM (error bars) of 10 or more cells per transfection from three independent experiments. Significant differences (unpaired Student's *t* test): *, $P < 0.0001$. (C and D) Immunofluorescence confocal images of COS-7 cells transfected with cDNA encoding S142A drebrin-YFP (C, green) or S142D drebrin-YFP (D, green) and labeled with phalloidin for F-actin (red) and antibody against α-actinin to label stress fibers (blue). S142A drebrin-YFP localizes to stress fibers (arrowheads) while S142D drebrin-YFP localizes to filopodia (arrows) and not to stress fibers (arrowheads). (E and F) Immunofluorescence confocal images of stage I cortical neurons (E) or growth cones from stage II/III cortical neurons (F) transfected with cDNA encoding S142A drebrin-YFP or S142D drebrin-YFP. Neurons were labeled with phalloidin for F-actin (red) and antibodies against GFP to visualize YFP-tagged drebrin (green) and drebrin (blue). S142A drebrin-YFP targets F-actin puncta (arrowheads) and actin arcs (curved arrows) in stage I neurons (E) and the Tzone in growth cones (F), whereas S142D drebrin-YFP localizes to F-actin puncta (arrowheads), filopodia (arrows), and actin arcs (curved arrows) in stage I neurons (E) and filopodia (arrows) in growth cones (F). (G and H) Fluorescence intensity in arbitrary units (AU) of F-actin (red), S142A drebrin-YFP (G, green), or S142D drebrin-YFP (H, green) and drebrin (blue) along the corresponding line plots shown in F (merge). S142A drebrin-YFP is mainly localized to the Tzone, whereas S142D drebrin-YFP is mainly localized to the base of the filopodium. Note that the drebrin level in the base of the filopodium is similar to that in the Tzone. (I and J) Electron micrographs of negatively stained F-actin from in vitro F-actin cosedimentation assays after addition of drebrin S142 mutant constructs. (I) After addition of S142A drebrin, thin, loose bundles of F-actin are visible, similar to those seen with wild-type drebrin (see Fig. 2 E). (J) After addition of S142D drebrin, thin, tight bundles of F-actin are visible. Bars: (A, D, and E) 5 µm; (C and F) 2.5 µm; (I) 100 nm; (J) 40 nm.

Chilton, 2010). Here we show that drebrin has two F-actin–binding domains—a CC and a Hel domain—that are adjacent to each other and located in the N-terminal half of the protein. These two domains can act cooperatively to bundle F-actin, and bundling is as efficient as that seen with fascin, a well-characterized F-actin–bundling protein. Fascin is probably a major F-actin–bundling protein in growth cone filopodia (Cohan et al., 2001) and therefore to what extent drebrin forms de novo bundles of F-actin or straddles preexisting F-actin bundles formed by fascin in growth cones has yet to be determined. Consistent with an

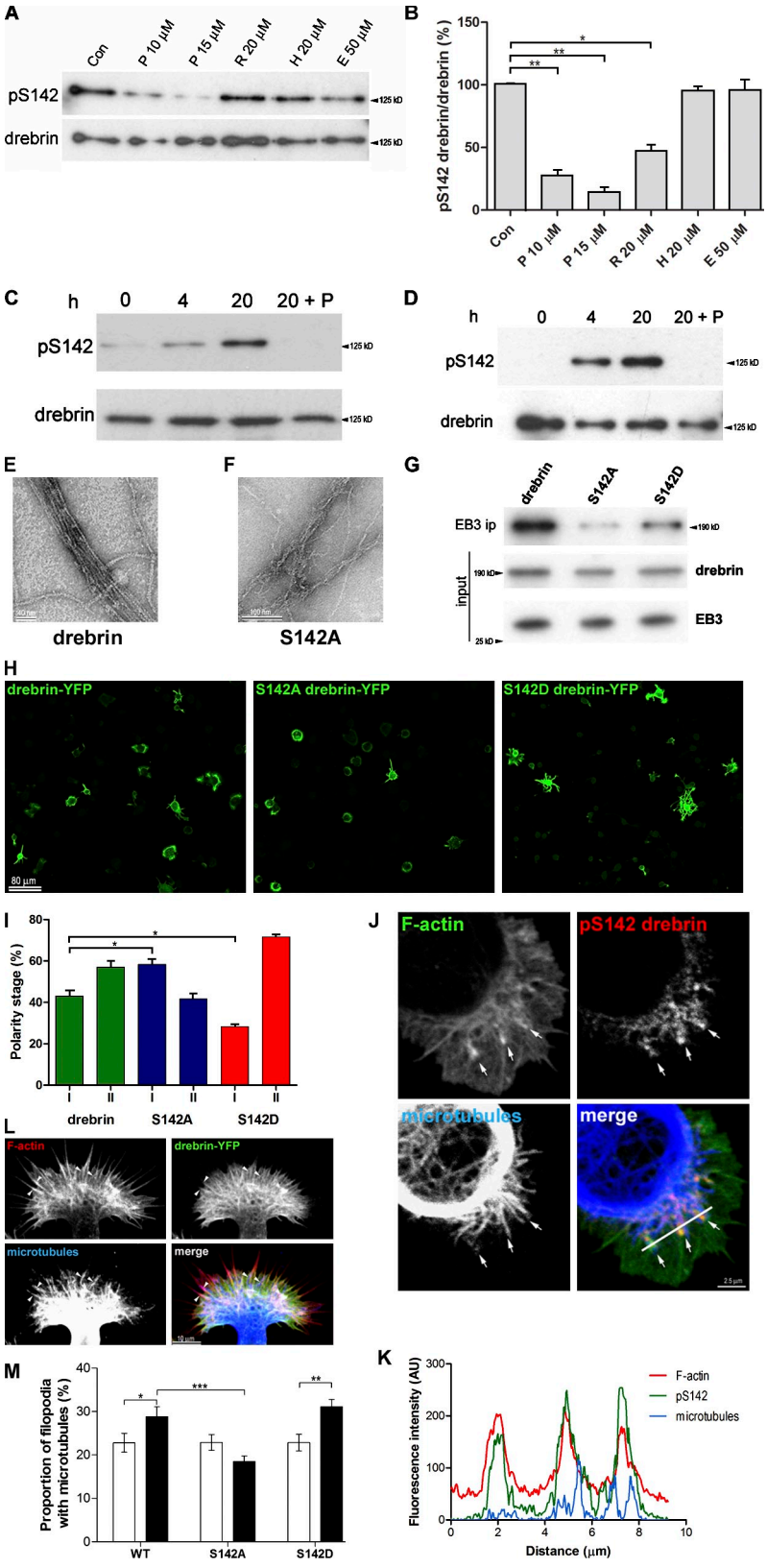

Figure 5. **Phosphorylation of drebrin at S142 by Cdk5 relieves the intramolecular inhibition of F-actin bundling.** (A and B) Inhibition of Cdk5, but not DYRK1A, reduces phosphorylation of drebrin at S142 in rat embryonic cortical cultures. Cultures were treated with vehicle (dimethyl sulfoxide, Con), the Cdk5 inhibitors purvalanol (P; 10 μM or 15 μM) or roscovitine (R; 20 μM), or the DYRK1A inhibitors harmine (H; 20 μM) or epigallocatechin-3-gallate (E; 50 μM) for 20 h, 2 h after plating. (A) Representative immunoblot of protein extracts from treated cultures probed with pAb pS142 and antibody to drebrin. Blots were also probed with a tubulin antibody (YL 1/2) to confirm equal loading (not depicted). (B) Densitometric quantification of the ratio of pS142 drebrin to drebrin from immunoblots of protein extracts from treated cultures. Error bars indicate SEM for three independent experiments. Significant differences (unpaired Student's *t* test): *, $P < 0.001$; **, $P < 0.0001$. (C and D) A cell extract from embryonic cortical cultures (C) or recombinant Cdk5/p35 (D) phosphorylate recombinant His-tagged drebrin at S142 in an in vitro kinase assay. Samples were removed from the kinase assay at the hours (h) indicated and immunoblotted with pAb pS142 (pS142) and antibody to drebrin. The Cdk5 inhibitor purvalanol (20 + P; 15 μM) completely blocked phosphorylation. The faint pS142 band at 0 h (C) is probably due to carryover of endogenous drebrin from the embryonic cortical culture extract. (E and F) Electron micrographs of negatively stained F-actin after addition of drebrin (E) or S142A drebrin (F) exposed to recombinant Cdk5/p35 in an in vitro F-actin cosedimentation assay. After addition of drebrin, a thin, tight bundle of F-actin is visible, indicating enhanced F-actin bundling compared with drebrin alone (compare with Fig. 2 E). After addition of S142A drebrin exposed to recombinant Cdk5/p35, thin, loose bundles of F-actin are visible, similar to those seen with wild-type drebrin (compare with Fig. 2 E). p35 was removed using glutathione beads after drebrin phosphorylation. Bars: (E) 40 nm; (F) 100 nm. (G) EB3 binds preferentially to S142-phosphorylated drebrin. EB3 immunoprecipitates (EB3 ip) of cell lysates from COS-7 cells expressing drebrin-YFP (drebrin), S142A drebrin-YFP (S142A), or S142D drebrin-YFP (S142D) were probed with drebrin antibody (mAb MX823). EB3 antibody efficiently immunoprecipitates drebrin-YFP and, to a lesser extent, S142D-drebrin-YFP, but not S142D drebrin-YFP. The levels of drebrin and EB3 in the inputs are similar. (H) Immunofluorescence confocal images of cortical neurons transfected with drebrin-YFP, S142A drebrin-YFP, or S142D drebrin-YFP and labeled with GFP antibody. Bar, 80 μm. (I) Quantitative analysis of the proportion of transfected neurons without neurites (stage I) and with neurites (stage II). Values are mean ± SEM (error bars) of 100 neurons per transfection from three independent experiments. Significant differences (one way ANOVA with Bonferroni post-hoc analysis): *, $P < 0.05$. (J) Immunofluorescence confocal images of a stage I cortical neuron commencing growth cone formation. The neuron was labeled with phalloidin for F-actin (green) and an antibody against pS142 drebrin (red) and mAb YL 1/2, which recognizes dynamic microtubules (blue). In the nascent growth cone, drebrin, phosphorylated at S142, colocalizes with bundles of F-actin (arrows). Dynamic microtubules enter the nascent growth cone from a circumferential bundle of microtubules in the cell body and pass alongside the drebrin/F-actin bundles in the nascent growth cone (arrows). (K) Fluorescence intensity in arbitrary units (AU) of F-actin (green), pS142 drebrin (red), and microtubules (blue) along the line plot shown in J (merge). F-actin and pS142 drebrin colocalize in three peaks while three microtubules (blue peaks) are located at the sides. (L) Immunofluorescence confocal images of a growth cone expressing drebrin-YFP used for the quantitative analysis of microtubule insertion into filopodia shown in M. The growth cone was labeled with phalloidin for F-actin (red) and mAb YL 1/2, which recognizes dynamic microtubules (blue). Moderately overexpressed drebrin extends into the base of the majority of filopodia, many of which are associated with dynamic microtubules (arrowheads). Bar, 10 μm. (M) Mutation of drebrin S142 to a phospho-dead (S142A) or phospho-mimetic (S142D) residue alters microtubule insertion into growth cone filopodia. Proportion of growth cone filopodia containing a microtubule in cultured embryonic cortical neurons transfected with wild-type (WT) drebrin-YFP, S142A drebrin-YFP (S142A), or S142D drebrin-YFP (S142D). White bars show nontransfected neurons. Significant differences (unpaired Student's *t* test): *, $P < 0.05$; **, $P < 0.001$; ***, $P < 0.0001$. Error bars indicate mean ± SEM.

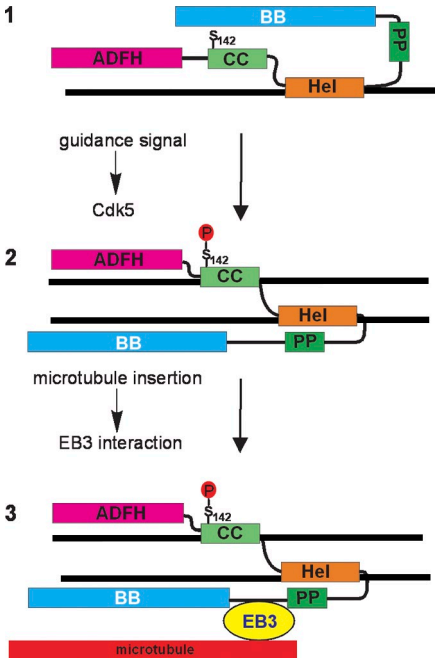

Figure 6. **Model of a molecular mechanism for coupling of F-actin to microtubules via an interaction between drebrin, phosphorylated at S142, and the +TIP protein EB3.** The diagram shows the domain structure of drebrin in the "closed" conformation, when the BB domain binds at the border between the ADFH and CC domains where S142 is located (1). In this conformation, drebrin can bind to F-actin but does not bundle or straddle preexisting F-actin bundles. One filopodial actin filament, represented by a black line, is also shown. Activation of Cdk5 by intracellular signaling pathways driven by axon guidance cues leads to S142 phosphorylation (2) and the consequent relief of the intramolecular occlusion of one F-actin–binding domain by the BB domain. This produces an "open" conformation, and drebrin now bundles F-actin, or straddles existing F-actin bundles, by cooperative binding of the CC and Hel domains. Drebrin in the "open" conformation and bound to F-actin at the base of filopodia is now in an appropriate state to interact with the +TIP protein EB3 located at the plus end of a microtubule (red line) entering the filopodium, and thereby couple F-actin to a microtubule (3).

F-actin bundling activity, it has previously been shown that overexpression of drebrin in growth cones increases F-actin levels (Mizui et al., 2009), and here we found that expression of drebrin in heterologous (COS-7) cells increased F-actin levels in these cells.

An intramolecular interaction represses F-actin bundling

We found evidence that the F-actin bundling activity of drebrin is repressed by an intramolecular interaction between the C-terminal BB domain and a region at the ADFH/CC border in the N-terminal half of the protein. This intramolecular repression of F-actin bundling is relieved by Cdk5 phosphorylation of a highly conserved serine, S142, that lies just upstream of the first actin-binding domain and eight amino acids downstream of the ADFH/CC border (Fig. 1 A). Our evidence includes results from comparative analysis of the F-actin binding and bundling of recombinant drebrin, S142 phosphorylated drebrin, and drebrin point-mutated at S142 to either alanine to produce a phospho-dead form, or aspartate to produce a phospho-mimetic. Because the BB domain binding site encompasses the ADFH/CC border and S142 is located eight amino acids downstream of the ADFH/CC border, S142 is appropriately located to influence BB binding. A functional interaction between the N- and C-terminal halves of drebrin has previously been inferred from in vivo transfection experiments with drebrin deletion mutants in chick oculomotor neurons (Dun et al., 2012).

A model for Cdk5 regulation of drebrin binding to filopodia

The findings reported here suggest that drebrin can bundle F-actin or bind to F-actin bundles in growth cone filopodia and that this activity is regulated by Cdk5, a kinase with important roles in neuronal migration (Ohshima et al., 1996), axon and dendrite growth (Nikolic et al., 1996), and growth cone pathfinding (Connell-Crowley et al., 2000). Cdk5 is also important in synaptic plasticity and is implicated in tau hyperphosphorylation in Alzheimer's disease (Su and Tsai, 2011). The regulated bundling of F-actin by drebrin has important implications for the organization of F-actin in growth cones and dendritic spines and thus in axon pathfinding and synaptic plasticity. Neuritogenesis and growth cone turning, a fundamental behavior during axon pathfinding, are both thought to depend on the coordinated interaction between dynamic microtubules and F-actin (Rodriguez et al., 2003). Our findings suggest a molecular mechanism to link filopodia stability and microtubule capture during neuritogenesis and growth cone pathfinding (Fig. 6). In growth cones, drebrin is predominantly located in the Tzone (Geraldo et al., 2008), where it is unphosphorylated at S142 and in the "closed" conformation (Fig. 6), presumably bound to single actin filaments. Upon Cdk5 phosphorylation, drebrin is converted to the "open" conformation by relieving the BB occlusion of an F-actin binding site and can now bundle F-actin de novo or relocate to the base of filopodia to stabilize the preexisting parallel bundle of F-actin forming the core of the filopodium. Thus, Cdk5 phosphorylation of drebrin might target it to the base of filopodia and position the protein appropriately for the capture of microtubules via EB3 (Fig. 6). This model is consistent with our findings, reported here, that drebrin phosphorylated at S142 is found in filopodia, but not in the Tzone, that mutating S142 to phospho-dead or phospho-mimetic forms respectively reduces or enhances microtubule coupling to F-actin in filopodia, and that EB3 preferentially binds to S142 phosphorylated drebrin, and with our previous observation that drebrin interacts with EB3 in growth cones only in filopodia (Geraldo et al., 2008). Whether drebrin–EB3 interactions are important for axon guidance is unresolved because, in a previous study of oculomotor neurons in the chick, knockdown of drebrin with shRNA produced no gross abnormalities in the projections of oculomotor axons to extraocular muscles (Dun et al., 2012). However, drebrin–EB3 interactions do seem to play a role in neuritogenesis because a dominant-negative EB3 construct interferes with neuritogenesis (Geraldo et al., 2008), and, as we show here, drebrin phospho-S142 mutants alter neuritogenesis.

Materials and methods

Antibodies/reagents

Mouse monoclonal antibody (mAb) against drebrin (clone MX823) was from Progen, rabbit polyclonal antibody (pAb) against EB3 (AB6033) was from EMD Millipore, rabbit pAb GFP (ab6556) was from Abcam, rat mAb

against tyrosinated α-tubulin (clone YL 1/2) was from AbD Serotec, rabbit pAb p35 (C-19) was from Santa Cruz Biotechnology, Inc., mouse mAb against α-actinin (clone BM-75.2) and goat anti–rabbit horseradish peroxidase–conjugated antibody were from Sigma-Aldrich, and His-tag mAb was from EMD Millipore. Alexa Fluor–conjugated antibodies, phalloidin, and Alexa Fluor 488–conjugated phalloidin were from Invitrogen. Horseradish peroxidase–conjugated secondary antibodies were from Dako. Purvalanol was from EMD Millipore, and all other chemicals were from Sigma-Aldrich.

Drebrin deletion constructs

Subcloning and PCR were performed using standard methods. Human drebrin E isoform (available from GenBank under accession no. D17530; GeneCopoeia) and drebrin deletion constructs were amplified by PCR with EcoRI and XhoI sites added to the 5′ and 3′ ends, respectively, using the following primers: forward primers for drebrin, ADFH, ADFH-CC, and ADFH-CC-Hel constructs, 5′-CTCGAATTCATGGCCGGCGTCAGCTTC-3′; for CC, CC-Hel, and CC-Hel-PP-BB constructs, 5′-CTCGAATTCATGGGGCTGGCGCGACTCT-3′; for Hel and Hel-PP-BB constructs, 5′-CTCGAATTCATGTTTGGTGACCATCGGGATGAG-3′; for PP-BB construct, 5′-CTCGAATTCATGCTGGATGAGGTCACCTCC-3′; for BB construct, 5′-CTCGAATTCATGCTGGCTGCTCCCGTGGAG-3′; reverse primers for drebrin, BB, PP-BB, Hel-PP-BB, and CC-Hel-PP-BB constructs, 3′-GCCTCGAGAAATCACCACCCTCGAAGCC-5′; for Hel, CC-Hel, and ADFH-CC-Hel constructs, 3′-GCCTCGAGAAGGCCCGCTCTATCTGCT-5′; for CC and ADFH-CC constructs, 3′-GCCTCGAGAGGATAGACTGCTCCTTCAACC-5′; and for ADFH construct, 3′-GCCTCGAGAAGTTAGAGAGCCGCTGCC-5′ (Sigma-Aldrich). PCR products were cloned into the pGEM-T Easy vector (Promega), excised by EcoRI and XhoI digestion, and inserted into EcoRI and SalI sites of the pEYFP-N1 vector (Takara Bio Inc.) and, for His-tagged deletion constructs, the pETDuet, pET30(+), or pET-24a vectors (EMD Millipore). Clones were verified by DNA sequencing.

Site-directed mutagenesis of drebrin at S142

The QuikChange XL Site-Directed Mutagenesis kit (Agilent Technology) was used to mutate the S142 site. Primer pairs used for the A142 mutation were: forward, 5′-GGCGCGACTCTCCGCCCCTGTGCTGCAC-3′; and reverse, 5′-GTGCAGCACAGGGGCGGAGAGTCGCGCC-3′. Primer pairs for the D142 mutation were: forward, 5′-GGCGCGACTCTCCGACCCTGTGCTGCAC-3′; and reverse, 5′-GTGCAGCACAGGGTCGGAGAGTCGCGCC-3′.

Expression and purification of recombinant proteins

Escherichia coli Rosetta (DE3) pLysS cells (EMD Millipore) transformed with cDNA encoding His-tagged drebrin or its deletion constructs were used for protein expression. Full-length drebrin and drebrin lacking the ADFH domain were grown to an OD600 of 0.5 in Luria-Bertani medium containing ampicillin and chloramphenicol at 37°C. Cells were induced to express protein by the addition of 1 mM IPTG, and incubation continued for a further 3 h at 28°C. For expression of drebrin deletion constructs, cells were grown to an OD600 of 0.9, induced with 1 mM IPTG, and incubated for 3 h at 37°C. Cultures were centrifuged at 6,000 *g* for 20 min and pellets were lysed in buffer containing 50 mM Tris, pH 8.0, 300 mM NaCl, 1 mg/ml lysozyme (Sigma-Aldrich), and bacterial protease inhibitors (Sigma-Aldrich). Lysates were spun for a further 20 min at 12,000 *g* and resulting supernatants were incubated overnight with Ni^{2+}-nitrilotriacetate (NTA) agarose beads (QIAGEN) at 4°C. Beads were either washed in PBS or purified protein was eluted with 500 mM imidazole and 300 mM NaCl in water containing protease and phosphatase inhibitors (Sigma-Aldrich), then concentrated in Nanosep centrifugal devices (Pall). Fascin was supplied by A. Jayo (Randall Division of Cell and Molecular Biophysics, King's College London, London, England, UK).

In vitro F-actin cosedimentation assays

Actin filaments were assembled by incubating ∼31.5 µM actin, prepared from rabbit skeletal muscle (Spudich and Watt, 1971), supplied by N. Elkhatib (Equipe de Migration et Invasion Cellulaire, Institut Curie, Paris, France) and E. Rostkova (Cardiovascular Department, King's College London), or human platelets (Cytoskeleton, Inc.), with 50 mM KCl, 2 mM $MgCl_2$, and 1 mM ATP at 4°C for 2 h. Actin filaments were pelleted by centrifugation for 90 min at 80,000 rpm (279,000 *g*) using an ultracentrifuge (Optima Max-XP; Beckman Coulter) and the TLA-100 rotor (Beckman Coulter). The pellet was resuspended in 67.5 µl of G buffer (2 mM Tris, pH 8.0, 0.2 mM ATP, 0.2 mM $CaCl_2$, and 0.5 mM DTT) and dialyzed overnight against G buffer at 4°C in a microdialysis button wrapped with dialysis membrane with a 12–14-kD cutoff. To remove contaminating F-actin bundling factors, F-actin was then centrifuged for 20 min at 12,100 *g* in a bench-top centrifuge (Eppendorf) to pellet F-actin bundles. The resulting supernatant was collected and then recentrifuged for the same time and speed until no F-actin appeared in the pellet, as confirmed by running the pellet fractions from each spin on an SDS-PAGE gel and staining with Imperial Protein Stain (Thermo Fischer Scientific). Binding and bundling cosedimentation assays were performed within 1 wk of F-actin preparation. 15 µM F-actin was incubated with a 7-µM concentration of the test protein and 2 µl of 10× KME buffer (500 mM KCl, 10 mM $MgCl_2$, 10 mM EGTA, and 100 mM imidazole, pH 7); water was added to bring the final volume to 20 µl. After incubation for 1 h at room temperature, the reaction mixture was first centrifuged at 12,100 *g* for 20 min to pellet F-actin bundles. The resulting supernatant was then centrifuged at 279,000 *g* for 90 min using a TLA-100 rotor to pellet single actin filaments. Proteins in pellets and supernatant were then separated on an SDS-PAGE gel (10 or 15% acrylamide) and stained using Imperial Protein Stain (Thermo Fischer Scientific). For competition assays, His-ADFH-CC was incubated overnight at 4°C with increasing concentrations of BB-His. F-actin was added the following morning and the assay was then continued as described in this paragraph.

For EM analysis of actin bundles, cosedimentation assays were prepared as described in the previous paragraph in a total volume of 15 µl. After 1 h of incubation, reactions were diluted 1:10 in KME buffer, and 3 µl aliquots were applied to Formvar- and carbon-coated 200 mesh copper grids prepared as in Jansen et al. (2011). After 30 s, grids were blotted to remove excess solution, stained with 1% (wt/vol) uranyl acetate for 1 min, blotted, and dried. Samples were viewed in a transmission electron microscope (Tecnai 20) at an accelerating voltage of 200 kV. Images were captured on a charge-coupled device camera (UltraScan Model 894 US1000; Gatan). Interfilament distances in actin bundles were calculated by using the intensity profile function on Elements (Nikon) and Excel (Microsoft) software, with distances between peaks on the intensity profile being taken as the distances between the centers of actin filaments. A minimum of 20 filament bundles from three independent experiments were analyzed at two locations along the bundle.

Mass spectrometry

Phosphorylation sites on drebrin were identified using tandem mass spectrometry (MS/MS) by Proteome Sciences, Institute of Psychiatry, King's College London. Proteins in the cosedimentation assay were separated by one-dimensional SDS-PAGE on 10% acrylamide minigels (Bio-Rad Laboratories). After Imperial Protein Coomassie blue staining (Thermo Fischer Scientific), the drebrin bands were excised from gels and digested with trypsin, and peptides were extracted from the gel pieces by a series of acetonitrile and aqueous washes. The extract was pooled with the initial supernatant and lyophilized. Each sample was then resuspended in 5 µl of 50 mM ammonium bicarbonate and analyzed by liquid chromatography MS/MS (LC-MS/MS). Chromatographic separations were performed using an EASY-NanoLC (Thermo Fischer Scientific). Peptides were resolved by reversed-phase chromatography on a 75 µm C18 EASY column using a linear gradient of acetonitrile in 0.1% formic acid. The gradient was delivered to elute the peptides at a flow rate of 300 nL/min over 60 min. The eluate was ionized by nanoelectrospray ionization using an Orbitrap Velos Pro running Xcaliber software (version 2.1.0 SP1 build 1160; (Thermo Fischer Scientific)) using Higher-energy C-trap Dissociation (HCD) for identification and collision-induced dissociation/multistage activation (CID/MSA) for optimized phosphopeptide analysis. The instrument was operated in automated data-dependent switching mode, selecting precursor ions based on their intensity for sequencing by HCD in a top 10 method. The MS/MS analyses were conducted using higher than normal collision energy profiles that were chosen based on the mass-to-charge ratio (m/z) and the charge state of the peptide. CID/MSA produces a combination of CID MS/MS spectra of the precursor ion with an additional CID fragmentation of the neutral loss ion of phosphoric acid (98 D) creating a loss of 49 D from the doubly charged precursor and a 32.7 D loss from the triply charged precursor without the need for isolation steps in the method. This method produces an increased amount of structurally informative fragment ions, represented in a composite spectrum, which includes information from multiple fragmentation events.

Phosphorylation of recombinant drebrin

Bacterially expressed recombinant His-tagged drebrin conjugated to nickel beads (QIAGEN) was incubated with a neonatal rat brain extract (Phelan and Gordon-Weeks, 1997; Geraldo et al., 2008), recombinant Cdk5/p35 (EMD Millipore), or a cell extract from 1 d in vitro embryonic cortical

neuronal cultures (see "Embryonic cortical cultures and transfections") in a kinase buffer containing phosphatase inhibitors (Scales et al., 2009) overnight at 30°C. Beads were washed three times in cold kinase buffer and resuspended in cold PBS. Because p35 bundles F-actin (He et al., 2011), we removed it using glutathione beads after phosphorylating drebrin. We confirmed this by immunoblotting with a rabbit p35 antibody (C-19; Santa Cruz Biotechnology, Inc.).

Production of phospho-specific drebrin antibodies

For the production of phospho-specific antibodies, two synthetic phosphopeptides, corresponding to amino acids 135–145 of rat drebrin, in which either S141 or S142 were phosphorylated (CNGLARLSSPVL), were synthesized and conjugated to keyhole limpet hemocyanin. Antisera—pAb pS141 and pAb pS142—were raised in rabbits (Eurogentec). Unphosphorylated peptide, of the same sequence, was also synthesized for column chromatography and peptide-inhibition studies (Eurogentec). Antisera were immunoaffinity purified using Pierce Sulfolink kits (Thermo Fischer Scientific), first on phosphopeptide columns and then on nonphosphopeptide columns, to separate non–phospho-specific antibodies. A synthetic phosphopeptide corresponding to amino acids 137–147 of rat drebrin (CLARLSSPVLHR; phosphorylated amino acid underlined) was synthesized and conjugated to keyhole limpet hemocyanin, and a mouse mAb pS142 was generated (Abmart).

Gel electrophoresis and immunoblotting

Protein samples were subjected to SDS-PAGE on 10% gels and Western blotted onto polyvinylidene difluoride (PVDF) membranes (Thermo Fischer Scientific). Membranes were blocked for 1 h at room temperature or overnight at 4°C in blocking buffer (5% [wt/vol] BSA and 0.1% [vol/vol] Tween 20 [Sigma-Aldrich] in TBS) and then probed for 1 h at room temperature or overnight at 4°C with primary antibody diluted in blocking buffer. Blots were washed three times in 5% BSA and 0.1% (vol/vol) Tween 20 in TBS, and incubated with peroxidase-conjugated secondary antibody (Sigma-Aldrich) diluted in blocking buffer for 1 h at room temperature. Blots were then washed three times in 5% BSA and 0.1% (vol/vol) Tween 20 in TBS, developed with enhanced chemiluminescent kits (EMD Millipore), and exposed to clear blue x-ray films (Photon Imaging Systems). Films were developed in a Fuji processor, scanned using a flatbed scanner (V500; Epsom), and analyzed with ImageJ software.

COS-7 cell culture and transfection

COS-7 cells were maintained at 37°C in DMEM (Gibco) containing 10% fetal bovine serum (Gibco) supplemented with 2 mM glutamine/100 IU/ml penicillin/100 IU ml^{-1} streptomycin (Sigma-Aldrich). Cells were plated onto glass coverslips for immunofluorescence microscopy and into six-well plates for biochemistry. Cells were transfected in DMEM medium using PolyJet (tebu-bio) and 0.5 µg of each DNA plasmid, according to the manufacturer's instructions. For controls, cells were treated as before, except DNA was omitted (mock transfection). 18 h after transfection, the medium was replaced with fresh medium, and the cells were fixed 24–48 h after transfection (see "Immunolabeling of cultures"). Immunoblotting showed that the level of expression in each transfection was equivalent.

EB3 immunoprecipitation

COS-7 cells were transfected with drebrin-YFP, S142A drebrin-YFP, or S142D drebrin-YFP constructs as described in the previous paragraph, and cells were lysed with RIPA buffer (20 mM Tris-HCl, pH 7.4,150 mM NaCl, 1 mM EGTA, 1 mM EDTA, 20 mM NaF, 1% [vol/vol] Triton X-100, 0.1% [wt/vol] SDS, 0.5% [vol/vol] sodium deoxycholate, and 1% [vol/vol] protease inhibitor cocktail [Sigma-Aldrich]). The lysate was precleared with Protein A agarose beads (Sigma-Aldrich) for 1 h at 4°C before incubating overnight with anti-EB3 antibody (EMD Millipore). Protein A agarose beads were added and allowed to incubate for 3 h at 4°C before washing extensively with PBS and collecting by centrifugation. Immunoblots of immunoprecipitates were probed with mAb MX823 (1:150).

BB domain pull-down assays

COS-7 cells were transfected with drebrin deletion constructs (see "COS-7 cell culture and transfection"), and cells were extracted with RIPA buffer containing a protease inhibitor cocktail (Thermo Fischer Scientific). His-tagged BB recombinant protein bound to NTA agarose beads (QIAGEN) was incubated with COS-7 cell extract overnight at 4°C and washed extensively in RIPA buffer by centrifugation.

Embryonic cortical cultures and transfections

Cerebral cortices were dissected from day 17–18 rat embryos and cells separated using a dissociation kit according to the manufacturer's instructions (Worthington Biochemical Corporation). Cells (10^5) were plated on 14-mm glass coverslips coated with poly-D-lysine (100 µg/ml; Sigma-Aldrich). For transfections, cells were resuspended in 250 µl of nucleofection solution (Ingenio) containing 2–4 µg of DNA and transferred to a cuvette. Program O-03 was used to electroporate the DNA into the cells. Cells were incubated at 37°C in 5% CO_2 in humidified air in Neurobasal medium (Gibco) supplemented with 2% (vol/vol) B27 supplement (Gibco), 2 mM glutamine/100 IU/ml penicillin/100 IU/ml streptomycin (Sigma-Aldrich) and 0.45% D−(+) glucose for 2–3 d. Neurons were then detached using trypsin-EDTA (0.25% in HBSS; Gibco) at 37°C for 5 min. Detached cells were pelleted by centrifugation for 5 min at 600 rpm, resuspended in PBS containing trypsin inhibitor (Sigma-Aldrich), and pelleted by centrifugation for 5 min at 1,000 rpm. The supernatant was removed and pelleted cells were resuspended in Neurobasal medium (Gibco) prepared as described in this paragraph and then replated onto 14-mm glass coverslips for immunolabeling.

Immunolabeling of cultures

COS-7 cells and cortical cultures were fixed for 10 min with 3% formaldehyde, 0.2% glutaraldehyde, and 0.2% Triton X-100 in PHEM buffer (Schliwa and van Blerkom, 1981) at 37°C. The fixative for cortical cultures also contained phalloidin (0.33 µM; Molecular Probes). COS-7 cells and cortical cultures were immunolabeled as described previously (Scales et al., 2009) with the following antibodies: mouse mAb to drebrin (clone MX823, 1:50; Progen), rabbit pAb to drebrin pS141 (1:100, CNGLARLSSPVL; phosphorylated amino acid underlined), or drebrin pS142 (1:100, CNGLARLSSPVL; phosphorylated amino acid underlined); mouse mAb to drebrin pS142 (1:100, CLARLSSPVLHR; phosphorylated amino acid underlined), rat mAb YL 1/2 (1:400, AbD Serotec), and rabbit pAb to GFP (1:1,000; Abcam), followed by incubation with the appropriate Alexa Fluor–conjugated secondary antibody (Invitrogen) and Alexa Fluor–conjugated phalloidin (Invitrogen). Labeled cultures were viewed using an confocal microscope (FluoView; Olympus) equipped with argon and HeNe lasers. Cells were imaged with a 100×/1.4 Plan-Apochromat oil-immersion objective lens and recorded at 1,024 × 1,024 pixels per image. Fluorescent images in TIFF format were manipulated using Photoshop (Adobe).

COS-7 cell filopodia were identified as that population of processes that extend as finger-like projections >1 µm from the cell edge and counted using Photoshop software. COS-7 cell perimeter was assessed by measuring the length of a line manually drawn around the cell edge using ImageJ software. To measure F-actin levels, single confocal optical sections of COS-7 cells taken close to the ventral surface, so as to include stress fibers, were collected using a 100× 1.3 NA oil-immersion objective lens. The integrated pixel intensity of the phalloidin signal, measured using ImageJ, was divided by the area of the cell in the optical section. Measurements were obtained from at least 10 cells per condition, chosen randomly from isolated cells in fixed cultures, from three independent experiments. To measure neuritogenesis in transfected neurons, embryonic cortical neuronal cultures were transfected for 2 d and then replated (see "Embryonic cortical cultures and transfections") to restart neuritogenesis. Cultures were fixed 1 h after replating and labeled with GFP antibody (Abcam), to identify transfected neurons, mAb YL 1/2 (SeroTec) to label microtubules in cell bodies and neurites, and with phalloidin to label F-actin. 100 transfected neurons, identified by GFP immunofluorescence, from each of three independent experiments were scored for neurite number. To count microtubule insertion into growth cone filopodia, microtubules, labeled with mAb YL/12 (AbD Serotec), and filopodia, labeled with phalloidin, were counted in 40 or more growth cones of transfected and nontransfected cultured neurons from three independent experiments.

Statistical analysis

Data were analyzed using GraphPad Prism 5 (GraphPad Software) and are expressed as mean ± SEM. Data were collected from three or more independent experiments. The unpaired Student's *t* test or analysis of variance (ANOVA) test was used for statistical analysis, whichever was appropriate. Differences between values were considered significant if $P < 0.05$.

In silico analysis

InterPro, Pfam, SMART, and PROSITE were used to analyze the human drebrin amino acid sequence for domains.

Online supplemental material

Fig. S1 shows that some drebrin deletion constructs induce filopodia, whereas others do not. Fig. S2 shows the F-actin–binding and –bundling

activities of drebrin constructs in in vitro F-actin cosedimentation assays and shows by negative-staining EM that the CC-Hel-PP-BB drebrin domain forms thin, loose bundles of F-actin. Fig. S3 shows by immunofluorescence that a pAb against pS141 drebrin does not label embryonic cortical neurons in culture. Table S1 shows drebrin phosphorylation sites from an F-actin cosedimentation assay identified by MS/MS. Table S2 shows a vertebrate evolutionary sequence comparison of the drebrin S142 site (S) and its flanking regions. Online supplemental material is available at http://www.jcb.org/cgi/content/full/jcb.201303005/DC1.

We are grateful to Anthony Brown for supplying centrifuge tubes bought on eBay, Britta Eickholt and Rita Hendricusdottir for help with raising a pS142 drebrin pAb, Nadia Elkhatib and Elena Rostkova for skeletal muscle actin, Asier Jayo for fascin, and Alice Warley in the King's Centre for Ultrastructural Imaging for help with EM. We thank the Eickholt laboratory for correcting some point mutations in drebrin cDNA.

This work was supported by grants from the Biotechnology and Biological Sciences Research Council, Medical Research Council, the Wellcome Trust, and Research into Aging. Sara Geraldo's PhD studentship was funded by Fundação para a Ciência e Tecnologia, Portugal.

Submitted: 1 March 2013
Accepted: 18 July 2013

References

Aoki, C., N. Kojima, N. Sabaliauskas, L. Shah, T.H. Ahmed, J. Oakford, T. Ahmed, H. Yamazaki, K. Hanamura, and T. Shirao. 2009. Drebrin a knockout eliminates the rapid form of homeostatic synaptic plasticity at excitatory synapses of intact adult cerebral cortex. *J. Comp. Neurol.* 517:105–121. http://dx.doi.org/10.1002/cne.22137

Ballif, B.A., J. Villén, S.A. Beausoleil, D. Schwartz, and S.P. Gygi. 2004. Phosphoproteomic analysis of the developing mouse brain. *Mol. Cell. Proteomics*. 3:1093–1101. http://dx.doi.org/10.1074/mcp.M400085-MCP200

Bazellières, E., D. Massey-Harroche, M. Barthélémy-Requin, F. Richard, J.P. Arsanto, and A. Le Bivic. 2012. Apico-basal elongation requires a drebrin-E-EB3 complex in columnar human epithelial cells. *J. Cell Sci.* 125:919–931. http://dx.doi.org/10.1242/jcs.092676

Biou, V., H. Brinkhaus, R.C. Malenka, and A. Matus. 2008. Interactions between drebrin and Ras regulate dendritic spine plasticity. *Eur. J. Neurosci.* 27:2847–2859. http://dx.doi.org/10.1111/j.1460-9568.2008.06269.x

Chew, C.S., C.T. Okamoto, X. Chen, and R. Thomas. 2005. Drebrin E2 is differentially expressed and phosphorylated in parietal cells in the gastric mucosa. *Am. J. Physiol. Gastrointest. Liver Physiol.* 289:G320–G331. http://dx.doi.org/10.1152/ajpgi.00002.2005

Cohan, C.S., E.A. Welnhofer, L. Zhao, F. Matsumura, and S. Yamashiro. 2001. Role of the actin bundling protein fascin in growth cone morphogenesis: localization in filopodia and lamellipodia. *Cell Motil. Cytoskeleton*. 48:109–120. http://dx.doi.org/10.1002/1097-0169(200102)48:2<109::AID-CM1002>3.0.CO;2-G

Collins, M.O., L. Yu, M.P. Coba, H. Husi, I. Campuzano, W.P. Blackstock, J.S. Choudhary, and S.G. Grant. 2005. Proteomic analysis of in vivo phosphorylated synaptic proteins. *J. Biol. Chem.* 280:5972–5982. http://dx.doi.org/10.1074/jbc.M411220200

Connell-Crowley, L., M. Le Gall, D.J. Vo, and E. Giniger. 2000. The cyclin-dependent kinase Cdk5 controls multiple aspects of axon patterning in vivo. *Curr. Biol.* 10:599–602. http://dx.doi.org/10.1016/S0960-9822(00)00487-5

Counts, S.E., B. He, M. Nadeem, J. Wuu, S.W. Scheff, and E.J. Mufson. 2012. Hippocampal drebrin loss in mild cognitive impairment. *Neurodegener. Dis.* 10:216–219. http://dx.doi.org/10.1159/000333122

Dotti, C.G., C.A. Sullivan, and G.A. Banker. 1988. The establishment of polarity by hippocampal neurons in culture. *J. Neurosci.* 8:1454–1468.

Dun, X.P., and J.K. Chilton. 2010. Control of cell shape and plasticity during development and disease by the actin-binding protein Drebrin. *Histol. Histopathol.* 25:533–540.

Dun, X.P., T. Bandeira de Lima, J. Allen, S. Geraldo, P. Gordon-Weeks, and J.K. Chilton. 2012. Drebrin controls neuronal migration through the formation and alignment of the leading process. *Mol. Cell. Neurosci.* 49:341–350. http://dx.doi.org/10.1016/j.mcn.2012.01.006

Geraldo, S., U.K. Khanzada, M. Parsons, J.K. Chilton, and P.R. Gordon-Weeks. 2008. Targeting of the F-actin-binding protein drebrin by the microtubule plus-tip protein EB3 is required for neuritogenesis. *Nat. Cell Biol.* 10:1181–1189. http://dx.doi.org/10.1038/ncb1778

Goode, B.L., A.A. Rodal, G. Barnes, and D.G. Drubin. 2001. Activation of the Arp2/3 complex by the actin filament binding protein Abp1p. *J. Cell Biol.* 153:627–634. http://dx.doi.org/10.1083/jcb.153.3.627

Grintsevich, E.E., V.E. Galkin, A. Orlova, A.J. Ytterberg, M.M. Mikati, D.S. Kudryashov, J.A. Loo, E.H. Egelman, and E. Reisler. 2010. Mapping of drebrin binding site on F-actin. *J. Mol. Biol.* 398:542–554. http://dx.doi.org/10.1016/j.jmb.2010.03.039

Harigaya, Y., M. Shoji, T. Shirao, and S. Hirai. 1996. Disappearance of actin-binding protein, drebrin, from hippocampal synapses in Alzheimer's disease. *J. Neurosci. Res.* 43:87–92. http://dx.doi.org/10.1002/jnr.490430111

Hatanpää, K., K.R. Isaacs, T. Shirao, D.R. Brady, and S.I. Rapoport. 1999. Loss of proteins regulating synaptic plasticity in normal aging of the human brain and in Alzheimer disease. *J. Neuropathol. Exp. Neurol.* 58:637–643. http://dx.doi.org/10.1097/00005072-199906000-00008

Hayashi, K., and T. Shirao. 1999. Change in the shape of dendritic spines caused by overexpression of drebrin in cultured cortical neurons. *J. Neurosci.* 19:3918–3925.

Hayashi, K., R. Ishikawa, R. Kawai-Hirai, T. Takagi, A. Taketomi, and T. Shirao. 1999. Domain analysis of the actin-binding and actin-remodeling activities of drebrin. *Exp. Cell Res.* 253:673–680. http://dx.doi.org/10.1006/excr.1999.4663

He, L., Z. Zhang, Y. Yu, S. Ahmed, N.S. Cheung, and R.Z. Qi. 2011. The neuronal p35 activator of Cdk5 is a novel F-actin binding and bundling protein. *Cell. Mol. Life Sci.* 68:1633–1643. http://dx.doi.org/10.1007/s00018-010-0562-9

Ishikawa, R., T. Sakamoto, T. Ando, S. Higashi-Fujime, and K. Kohama. 2003. Polarized actin bundles formed by human fascin-1: their sliding and disassembly on myosin II and myosin V in vitro. *J. Neurochem.* 87:676–685. http://dx.doi.org/10.1046/j.1471-4159.2003.02058.x

Ivanov, A., M. Esclapez, and L. Ferhat. 2009. Role of drebrin A in dendritic spine plasticity and synaptic function: Implications in neurological disorders. *Commun. Integr. Biol.* 2:268–270. http://dx.doi.org/10.4161/cib.2.3.8166

Jansen, S., A. Collins, C. Yang, G. Rebowski, T. Svitkina, and R. Dominguez. 2011. Mechanism of actin filament bundling by fascin. *J. Biol. Chem.* 286:30087–30096. http://dx.doi.org/10.1074/jbc.M111.251439

Jaworski, J., L.C. Kapitein, S.M. Gouveia, B.R. Dortland, P.S. Wulf, I. Grigoriev, P. Camera, S.A. Spangler, P. Di Stefano, J. Demmers, et al. 2009. Dynamic microtubules regulate dendritic spine morphology and synaptic plasticity. *Neuron*. 61:85–100. http://dx.doi.org/10.1016/j.neuron.2008.11.013

Keon, B.H., P.T. Jedrzejewski, D.L. Paul, and D.A. Goodenough. 2000. Isoform specific expression of the neuronal F-actin binding protein, drebrin, in specialized cells of stomach and kidney epithelia. *J. Cell Sci.* 113:325–336.

Kessels, M.M., A.E. Engqvist-Goldstein, and D.G. Drubin. 2000. Association of mouse actin-binding protein 1 (mAbp1/SH3P7), an Src kinase target, with dynamic regions of the cortical actin cytoskeleton in response to Rac1 activation. *Mol. Biol. Cell*. 11:393–412. http://dx.doi.org/10.1091/mbc.11.1.393

Kobayashi, R., Y. Sekino, T. Shirao, S. Tanaka, T. Ogura, K. Inada, and M. Saji. 2004. Antisense knockdown of drebrin A, a dendritic spine protein, causes stronger preference, impaired pre-pulse inhibition, and an increased sensitivity to psychostimulant. *Neurosci. Res.* 49:205–217. http://dx.doi.org/10.1016/j.neures.2004.02.014

Kojima, N., K. Hanamura, H. Yamazaki, T. Ikeda, S. Itohara, and T. Shirao. 2010. Genetic disruption of the alternative splicing of drebrin gene impairs context-dependent fear learning in adulthood. *Neuroscience*. 165:138–150. http://dx.doi.org/10.1016/j.neuroscience.2009.10.016

Lappalainen, P., M.M. Kessels, M.J. Cope, and D.G. Drubin. 1998. The ADF homology (ADF-H) domain: a highly exploited actin-binding module. *Mol. Biol. Cell*. 9:1951–1959. http://dx.doi.org/10.1091/mbc.9.8.1951

Larbolette, O., B. Wollscheid, J. Schweikert, P.J. Nielsen, and J. Wienands. 1999. SH3P7 is a cytoskeleton adapter protein and is coupled to signal transduction from lymphocyte antigen receptors. *Mol. Cell. Biol.* 19:1539–1546.

Lee, D., and C. Aoki. 2012. Presenilin conditional double knockout mice exhibit decreases in drebrin a at hippocampal CA1 synapses. *Synapse*. 66:870–879. http://dx.doi.org/10.1002/syn.21578

Mizui, T., N. Kojima, H. Yamazaki, M. Katayama, K. Hanamura, and T. Shirao. 2009. Drebrin E is involved in the regulation of axonal growth through actin-myosin interactions. *J. Neurochem.* 109:611–622. http://dx.doi.org/10.1111/j.1471-4159.2009.05993.x

Nikolic, M., H. Dudek, Y.T. Kwon, Y.F. Ramos, and L.H. Tsai. 1996. The cdk5/p35 kinase is essential for neurite outgrowth during neuronal differentiation. *Genes Dev.* 10:816–825. http://dx.doi.org/10.1101/gad.10.7.816

Ohshima, T., J.M. Ward, C.G. Huh, G. Longenecker, H.C. Veeranna, H.C. Pant, R.O. Brady, L.J. Martin, and A.B. Kulkarni. 1996. Targeted disruption

of the cyclin-dependent kinase 5 gene results in abnormal corticogenesis, neuronal pathology and perinatal death. *Proc. Natl. Acad. Sci. USA*. 93:11173–11178. http://dx.doi.org/10.1073/pnas.93.20.11173

Phelan, P., and P.R. Gordon-Weeks. 1997. Isolation of synaptosomes, growth cones and their subcelllular components. Neurochemistry, A Practical Approach. A.J. Turner and H.S. Bachelard, editors. London, IRL Press: 1–38.

Quintero-Monzon, O., A.A. Rodal, B. Strokopytov, S.C. Almo, and B.L. Goode. 2005. Structural and functional dissection of the Abp1 ADFH actin-binding domain reveals versatile in vivo adapter functions. *Mol. Biol. Cell*. 16:3128–3139. http://dx.doi.org/10.1091/mbc.E05-01-0059

Rodriguez, O.C., A.W. Schaefer, C.A. Mandato, P. Forscher, W.M. Bement, and C.M. Waterman-Storer. 2003. Conserved microtubule-actin interactions in cell movement and morphogenesis. *Nat. Cell Biol.* 5:599–609. http://dx.doi.org/10.1038/ncb0703-599

Scales, T.M., S. Lin, M. Kraus, R.G. Goold, and P.R. Gordon-Weeks. 2009. Nonprimed and DYRK1A-primed GSK3 beta-phosphorylation sites on MAP1B regulate microtubule dynamics in growing axons. *J. Cell Sci.* 122:2424–2435. http://dx.doi.org/10.1242/jcs.040162

Schliwa, M., and J. van Blerkom. 1981. Structural interaction of cytoskeletal components. *J. Cell Biol.* 90:222–235. http://dx.doi.org/10.1083/jcb.90.1.222

Shim, K.S., and G. Lubec. 2002. Drebrin, a dendritic spine protein, is manifold decreased in brains of patients with Alzheimer's disease and Down syndrome. *Neurosci. Lett.* 324:209–212. http://dx.doi.org/10.1016/S0304-3940(02)00210-0

Shirao, T., N. Kojima, and K. Obata. 1992. Cloning of drebrin A and induction of neurite-like processes in drebrin-transfected cells. *Neuroreport*. 3:109–112. http://dx.doi.org/10.1097/00001756-199201000-00029

Shirao, T., K. Hayashi, R. Ishikawa, K. Isa, H. Asada, K. Ikeda, and K. Uyemura. 1994. Formation of thick, curving bundles of actin by drebrin A expressed in fibroblasts. *Exp. Cell Res.* 215:145–153. http://dx.doi.org/10.1006/excr.1994.1326

Songyang, Z., K.P. Lu, Y.T. Kwon, L.H. Tsai, O. Filhol, C. Cochet, D.A. Brickey, T.R. Soderling, C. Bartleson, D.J. Graves, et al. 1996. A structural basis for substrate specificities of protein Ser/Thr kinases: primary sequence preference of casein kinases I and II, NIMA, phosphorylase kinase, calmodulin-dependent kinase II, CDK5, and Erk1. *Mol. Cell. Biol.* 16:6486–6493.

Spudich, J.A., and S. Watt. 1971. The regulation of rabbit skeletal muscle contraction. I. Biochemical studies of the interaction of the tropomyosin-troponin complex with actin and the proteolytic fragments of myosin. *J. Biol. Chem.* 246:4866–4871.

Su, S.C., and L.H. Tsai. 2011. Cyclin-dependent kinases in brain development and disease. *Annu. Rev. Cell Dev. Biol.* 27:465–491. http://dx.doi.org/10.1146/annurev-cellbio-092910-154023

Xu, W., and M. Stamnes. 2006. The actin-depolymerizing factor homology and charged/helical domains of drebrin and mAbp1 direct membrane binding and localization via distinct interactions with actin. *J. Biol. Chem.* 281:11826–11833. http://dx.doi.org/10.1074/jbc.M510141200